2011 50th IEEE Conference on Decision and Control and
European Control Conference (CDC-ECC)
Orlando, FL, USA, December 12-15, 2011

FWD Vehicle Drifting Control: The Handbrake-Cornering Technique

Efstathios Velenis

Abstract— **Race drivers employ expert techniques to exploit the limits of the vehicle performance. In particular, rally driving techniques involve vehicle cornering at high sideslip angles (drifting), and hence operation of the vehicle beyond the stable limits enforced by stability control systems. In this work we study drifting techniques applicable to Front-Wheel-Drive (FWD) drive-train configurations. We present data collected during the execution of handbrake-cornering maneuvers by an expert driver in a FWD vehicle. Consequently, we calculate cornering equilibria using a vehicle model with driven front wheels, and rear wheels "locked" at zero angular rate under application of the handbrake. A controller is designed to stabilize the vehicle with respect to the calculated equilibria, using steering and drive/brake torque control inputs. The controller is implemented in simulation to demonstrate the stabilization of unstable drifting steady-states.**

I. Introduction

The study of vehicle operation near the limits of its handling capacity, that is, with the tires operating near the adhesion limit, was initially motivated by the needs of the motorsport industry. Lap-time simulation algorithms have been developed, aiming to provide a low cost alternative to track testing during vehicle development and tuning. Casanova et al, for instance, developed nonlinear programming optimization techniques, incorporating rich dynamic models of the vehicle describing its transient behavior, to solve the minimum time problem over closed Formula 1 type of racing circuits [1], [2]. A similar nonlinear optimization approach was used in the mathematical analysis of rally driving techniques by Velenis et al. [3], [4]. Rally driving techniques clearly involve operation of the vehicle outside the stable operation envelope enforced by modern active safety systems, such as the Electronic Stability Control, as the vehicle reaches extreme sideslip angles and the tires operate in their nonlinear region. It is envisioned that the deeper understanding of the limit behavior of the vehicle will contribute to improvements on the existing and future active safety systems. The analysis in the above references provided a significant understanding of the optimality properties of limit driving techniques. However, the numerical optimization approach involves intense computations, and hence in is not implementable in real time and in the presence of uncertainties and disturbances.

Several studies have contributed towards the characterization and stabilization of steady-state cornering near the limit of handling. Ono et al. derived steady-state cornering equilibria with the tires operating in their full linear and nonlinear range and designed a robust stabilizing steering controller, under the assumption of negligible longitudinal forces at the tires [5]. The stability of steady-state cornering at high-sideslip angles (drifting) using a rich four-wheel rear-wheel-drive (RWD) vehicle model was discussed in [6]. Stabilization of drifting equilibria appeared in [7], [8], [9] and [10]. In [7], [8] a sliding mode controller, using independent front and rear wheel torque inputs and fixed steering angle, was designed to stabilize a single-track vehicle model with respect to drifting equilibria. In [9] a linear steering controller was implemented in a RWD autonomous vehicle performing a steady-state drifting manoeuvre. The steering controller design in [9] considered the lateral dynamics of a single-track model, while a separate controller was implemented to regulate the speed of the vehicle to the desired steady-state value. Finally, in [10] a coordinated steering and drive torque controller was designed to stabilize a four-wheel model of a RWD vehicle with respect to drifting cornering equilibria.

In this work we present a controller to stabilize a FWD vehicle with respect to high sideslip equilibria, using coordinated lateral (steering) and longitudinal (drive/brake torque) control inputs. While RWD drifting is stabilized using throttle and steering inputs [6], [10], FWD drifting is induced using the handbrake-cornering technique. First, we present data collected during the execution of handbrake-cornering maneuvers by an expert driver and discuss the correlation between driver inputs and vehicle response. We then introduce a vehicle model and calculate the steady-state tire friction forces and the associated drive/brake torque and steering angle control inputs corresponding to handbrake-cornering equilibria, i.e. with the rear wheel locked. A linear controller is designed to stabilize the vehicle with respect to drifting equilibria using front wheel steering angle and wheel angular rate, with the rear wheel speed fixed at zero. A back-stepping control scheme is then employed providing the drive torque input necessary to regulate the front wheel speed to the value dictated by the above linear controller, and the rear brake torque to maintain wheel lock. Finally, the control scheme is implemented in simulation to demonstrate the stabilization of unstable drifting equilibria.

II. Handbrake-Cornering Data Analysis

In this section we present and analyse data of driver control inputs and corresponding vehicle response collected during the execution of handbrake-cornering maneuvers by an experienced rally driver. The data collection took place at the facilities of the Bill Gwynne Rally School in Brackley, UK, using a rally-race prepared 2006 Ford Fiesta with a FWD transmission (Fig. 1). The Anti-Lock-Brake system

E. Velenis (corresponding author) is with the School of Engineering and Design, Brunel University, Uxbridge, Middlesex, UB8-3PH, UK, Email: efstathios.velenis@brunel.ac.uk

978-1-61284-799-3/11/$26.00 ©2011 IEEE

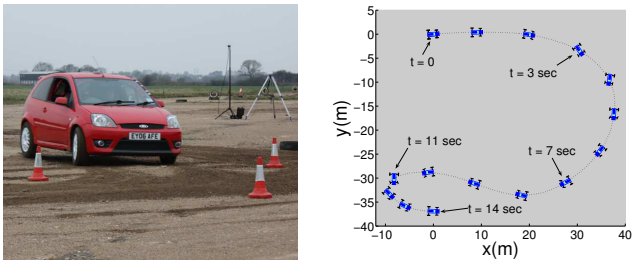

Fig. 1. *The test vehicle during data collection and vehicle trajectory data..*

was deactivated and the handbrake was integrated in the hydraulic brakes circuit, engaging the rear brakes only. The driver executed handbrake-cornering maneuvers on a gravel surface, negotiating a right turn of approximately $15\,\mathrm{m}$ of radius, followed by a tight left "hairpin" (180 deg) corner around a cone. Data of the vehicle speed V, sideslip angle β, yaw rate $\dot{\psi}$ and path curvature k are shown in Fig. 2. In the same figure individual wheel speeds $\omega_{ij},\ i = F\,(\mathrm{Front}), R\,(\mathrm{Rear}),\ j = L\,(\mathrm{Left}), R\,(\mathrm{Right})$, steering angle δ of the front wheels, and normalized throttle pedal position and front and rear brake pressure are shown. The vehicle sideslip and yaw rate are positive along the counterclockwise direction. Positive values of the steering angle δ correspond to turning left. In order to assess the vehicle's under/over-steer behavior we present the instantaneous kinematic path curvature and kinematic yaw rate of a neutral-steer bicycle model [11] alongside the corresponding data. The vehicle trajectory is shown in Fig. 1.

During $0.5 \leq t \leq 2\,\mathrm{sec}$ the vehicle accelerated under the application of throttle, while the driver applied an increasing steering input to the right. We observe that the vehicle under-steered during this interval, as the yaw rate and path curvature are both lower in magnitude than the corresponding kinematic values. To remedy the vehicle under-steer, the driver applied a handbrake command between $1.5 \leq t \leq 3\,\mathrm{sec}$, as shown by the increase of the rear brake pressure, while the front brake pressure remained at zero. Consequently, the rear wheel angular rates were reduced at a high rate, with the rear-right wheel locking. During this interval the driver also came off the throttle and continued to steer to the right. The resulting vehicle response during $2 \leq t \leq 4\,\mathrm{sec}$ is characterized by a decrease of vehicle speed, and an increase of the magnitude of sideslip and yaw rate. In particular, between $3 \leq t \leq 4\,\mathrm{sec}$ the yaw rate and path curvature magnitudes were higher than the kinematic ones, indicating vehicle over-steer. Hence, the handbrake-cornering technique can be used to eliminate under-steer during cornering. In accordance to the combined longitudinal and lateral motion of tires [12], by applying the handbrake and locking the rear wheels the driver achieves to drastically decrease the cornering (lateral) forces of the rear tires. The decrease of the stabilizing rear cornering forces result in an increase of the resultant yaw moment, which is experienced as an increase in the vehicle yaw rate and sideslip angle. After releasing the handbrake, the driver counter-steered

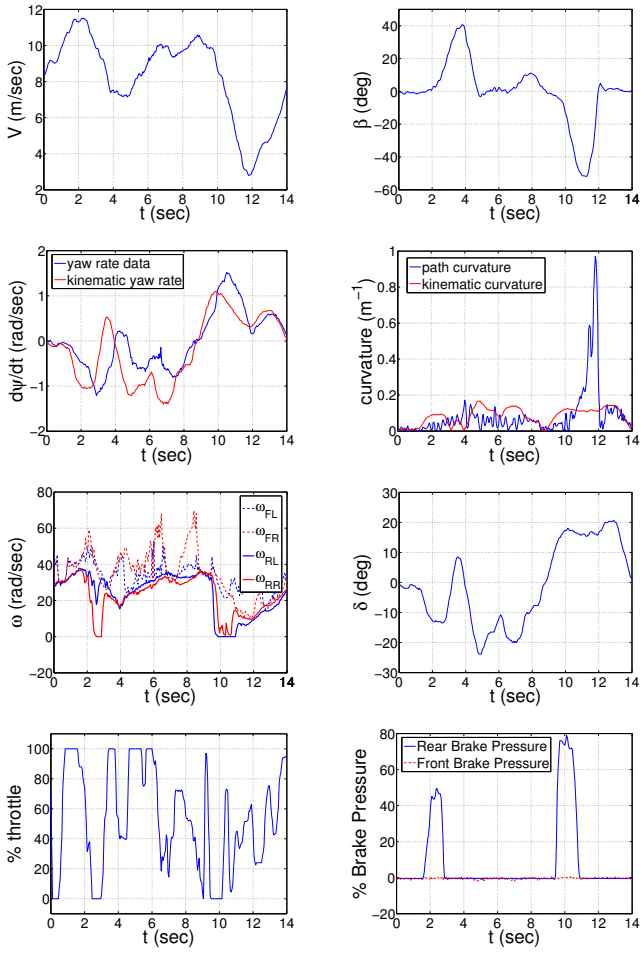

Fig. 2. *Handbrake-Cornering data.*

(steered to the opposite direction of the corner) and applied throttle, to limit the vehicle over-steer, in accordance to the observations in [3]. The change of sign in the kinematic yaw rate is due to the driver counter-steering.

The driver applied a handbrake command during $9.5 \leq t \leq 11\,\mathrm{sec}$, while negotiating the left "hairpin" turn. The result was, once again, an increase in vehicle sideslip and yaw rate. The path curvature reached an instantaneous magnitude of approximately $1\,\mathrm{m}^{-1}$, which corresponds to an instantaneous cornering radius of $1\,\mathrm{m}$. In low speeds the test vehicle can achieve a minimum turning radius of $4.5\,\mathrm{m}$ under the application of full-lock of the steering wheel ($30\,\mathrm{deg}$). Hence, the handbrake-cornering technique can be used to further decrease the cornering radius. We observe, that during the "hairpin" corner, the driver did not counter-steer, following the release of the handbrake. Instead, he applied throttle and progressively reduced the steering command to bring the vehicle back to a straight line acceleration.

In the next sections, we extend the approach of [8], [10] to explore the existence of steady-state handbrake equilibria. We enforce FWD drive-train configuration and rear wheel lock during cornering, to emulate the cornering maneuvers described above.

III. Vehicle Model

The equations of motion of the single-track model (Fig. 3) are as follows [7]:

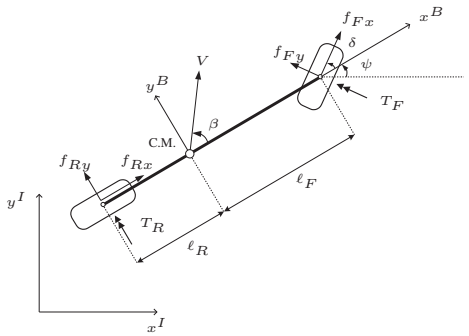

Fig. 3. *Single-track vehicle model.*

$$\begin{aligned} m\dot{V} &= f_{Fx}\cos(\delta-\beta) - f_{Fy}\sin(\delta-\beta) \\ &+ f_{Rx}\cos\beta + f_{Ry}\sin\beta, \quad (1) \\ \dot{\beta} &= 1/(mV)\left[f_{Fx}\sin(\delta-\beta) + f_{Fy}\cos(\delta-\beta)\right. \\ &- \left. f_{Rx}\sin\beta + f_{Ry}\cos\beta\right] - \dot{\psi}, \quad (2) \\ I_z\ddot{\psi} &= \left(f_{Fy}\cos\delta + f_{Fx}\sin\delta\right)\ell_F - f_{Ry}\ell_R, \quad (3) \\ I_{wi}\dot{\omega}_i &= T_i - f_{ix}r_i, \qquad i = F, R \quad (4) \end{aligned}$$

In the above equations m is the vehicle's mass, I_z is the polar moment of inertia of the vehicle, r_i is the radius of each of the front and rear wheels, I_{wi} is the moment of inertia of each wheel, and ℓ_F, ℓ_R is the distance of the center of mass (C.M.) from the front and rear axles respectively. V is the vehicle velocity, ψ is the yaw angle of the vehicle, β is the sideslip angle at the C.M. By f_{ij} $(i = F, R$ and $j = x, y)$ we denote the longitudinal and lateral tire friction forces at the front and rear wheels, respectively. T_i is the drive/brake torque at each of the wheels, and δ is the steering angle of the front wheel.

In [12] the theoretical longitudinal and lateral slip quantities are defined, respectively, as:

$$s_{ix} = \frac{V_{ix} - \omega_i r_i}{\omega_i r_i}, \qquad s_{iy} = \frac{V_{iy}}{\omega_i r_i} = (1 + s_{ix})\tan\alpha_i. \quad (5)$$

The tire frame components of the vehicle body velocity vector at the front and rear axles are V_{ij}, $(i = F, R,\ i = x, y)$ and given by:

$$V_{Fx} = V\cos(\beta-\delta) + \dot{\psi}\ell_f\sin\delta,\ V_{Rx} = V\cos(\beta),$$
$$V_{Fy} = V\sin(\beta-\delta) + \dot{\psi}\ell_f\cos\delta,\ V_{Ry} = V\sin(\beta) - \dot{\psi}\ell_R.$$

The slip angle at each wheel is given by $\tan\alpha_i = V_{iy}/V_{ix}$. The resultant slip at each tire is defined by $s_i = \sqrt{s_{ix}^2 + s_{iy}^2}$.

Assuming linear dependence of the tire friction forces on the tire vertical force, we obtain

$$\mu_i = f_i/f_{iz}, \quad \mu_{ij} = f_{ij}/f_{iz}, \qquad i = F, R, \quad j = x, y, \quad (6)$$

where $f_i = \sqrt{f_{ix}^2 + f_{iy}^2}$ is the resultant friction force at each tire, μ_i is the resultant friction coefficient, μ_{ij} are the longitudinal and lateral friction coefficients, and f_{iz} are the vertical forces at the front and rear tires.

We calculate the resultant friction coefficient using Pacejka's "magic formula" (MF) [12] as follows:

$$\mu_i(s_i) = \mathrm{MF}(s_i) = D\ \sin(C\ \mathrm{atan}(B\ s_i)). \quad (7)$$

Assuming symmetric tire characteristics, with respect to the longitudinal and lateral directions, the resultant friction force for each tire lies within the so-called friction circle:

$$\mu_{ij} = -(s_{ij}/s_i)\mu(s_i). \quad (8)$$

Neglecting the suspension dynamics the front and rear axle normal forces are given by:

$$\begin{aligned} f_{Fz} &= \frac{\ell_R mg - hmg\mu_{Rx}}{L + h\left(\mu_{Fx}\cos\delta - \mu_{Fy}\sin\delta - \mu_{Rx}\right)}, \quad (9) \\ f_{Rz} &= mg - f_{Fz}. \quad (10) \end{aligned}$$

where h is the height of C.M. from the road surface, and L is the wheelbase of the vehicle.

IV. Steady-State Handbrake-Cornering

Steady-state cornering is characterized by a trajectory of constant radius, negotiated at a constant speed, and constant yaw rate and slip angle:

$$R = R^{\mathrm{ss}},\ V = V^{\mathrm{ss}},\ \dot{\psi} = \dot{\psi}^{\mathrm{ss}} = \frac{V^{\mathrm{ss}}}{R^{\mathrm{ss}}},\ \beta = \beta^{\mathrm{ss}}.$$

Under steady-state conditions the wheel angular rates, tire longitudinal and lateral slip quantities and forces, and steering and drive/brake torque inputs are also constant

$$\omega_i = \omega_i^{\mathrm{ss}},\ s_{ij} = s_{ij}^{\mathrm{ss}},\ f_{ij} = f_{ij}^{\mathrm{ss}},\ \delta = \delta^{\mathrm{ss}},\ T_i = T_i^{\mathrm{ss}}.$$

During handbrake-cornering the rear wheels of the vehicle are locked, hence we enforce

$$\omega_R^{\mathrm{ss}} = 0, \quad (11)$$

which implies

$$s_{Rx}^{\mathrm{ss}} = \lim_{\omega_R\to 0}(s_{Rx}) = +\infty,\ s_R^{\mathrm{ss}} = \lim_{\omega_R\to 0}(s_R) = +\infty.$$

The resultant steady-state rear wheel tire force coefficient is then given by

$$\mu_R^{\mathrm{ss}} = \lim_{\omega_R\to 0}\mathrm{MF}(s_R) = D\ \sin(C\pi/2). \quad (12)$$

With $\dot{\psi}^{\mathrm{ss}} = V^{\mathrm{ss}}/R^{\mathrm{ss}}$, the steady-state slip angle at the rear wheel can be expressed as

$$\tan\alpha_R^{\mathrm{ss}} = V_{Ry}^{\mathrm{ss}}/V_{Rx}^{\mathrm{ss}} = V^{\mathrm{ss}}\tan\beta^{\mathrm{ss}} - \frac{\ell_R}{R^{\mathrm{ss}}\cos\beta^{\mathrm{ss}}}. \quad (13)$$

It can be shown that with $s_{Rx}^{\mathrm{ss}} \to +\infty$, the rear tire lateral force coefficient is given by

$$\mu_{Ry}^{\mathrm{ss}} = -\frac{\tan\alpha_{\mathrm{R}}^{\mathrm{ss}}}{\sqrt{1+\tan^2\alpha_R^{\mathrm{ss}}}}\mu_R^{\mathrm{ss}}. \quad (14)$$

The results from [7], [8] can now be applied to complete the calculation of the equilibrium states and control inputs. In particular, under steady-state conditions, the following

expressions for the steady-state normal forces and rear lateral force were derived:

$$f_{Rz}^{\rm ss} = \frac{mg\ell_F - mh(V^{\rm ss})^2 \sin\beta^{\rm ss}/R^{\rm ss}}{\ell_F+\ell_R}, \quad (15)$$

$$f_{Fz}^{\rm ss} = \frac{mg\ell_R + mh(V^{\rm ss})^2 \sin\beta^{\rm ss}/R^{\rm ss}}{\ell_F+\ell_R}, \quad (16)$$

$$f_{Ry}^{\rm ss} = \mu_{Ry}^{\rm ss} f_{Rz}^{\rm ss} = \frac{m(V^{\rm ss})^2}{R^{\rm ss}} \cos\beta^{\rm ss} \frac{\ell_F}{\ell_F+\ell_R}. \quad (17)$$

Substituting $\mu_{Ry}^{\rm ss}$ from (14), $f_{Rz}^{\rm ss}$ from (15), $\tan\alpha_R^{\rm ss}$ from (13) and $\mu_R^{\rm ss}$ from (12) into (17), one can numerically solve equation (17) to find the steady-state vehicle velocity $V^{\rm ss}$ for a given pair $(R^{\rm ss}, \beta^{\rm ss})$. Consequently, all of the rear wheel steady-state slip quantities s_{Rx}, s_{Ry}, and forces f_{Rx}, f_{Ry} and f_{Rz} can be calculated for a given pair $(R^{\rm ss}, \beta^{\rm ss})$.

As demonstrated in [7], [8] the resultant front axle friction force under steady-state conditions is given by:

$$f_F^{\rm ss} = \left(\frac{m^2(V^{\rm ss})^4}{(R^{\rm ss})^2} + (f_{Rx}^{\rm ss})^2 + (f_{Ry}^{\rm ss})^2 + \right.$$
$$\left. + \; 2\frac{m(V^{\rm ss})^2}{R^{\rm ss}} \left(f_{Rx}^{\rm ss}\sin\beta^{\rm ss} - f_{Ry}^{\rm ss}\cos\beta^{\rm ss} \right) \right)^{\frac{1}{2}},$$

whereas the front axle normal load from (16). Hence the front wheel resultant force coefficient μ_F and resultant slip s_F are given by equations (6) and (7) respectively. Applying the friction circle equation (8) and the friction coefficient definition (6) at the front axle forces in equations (1)-(2), under steady-state conditions, results in:

$$\frac{(V^{\rm ss})^2}{R^{\rm ss}} = \frac{(f_F^{\rm ss}/s_F^{\rm ss})(s_{Fx}^{\rm ss}\cos\delta^{\rm ss} - s_{Fy}^{\rm ss}\sin\delta^{\rm ss}) - f_{Rx}^{\rm ss}}{m\sin\beta^{\rm ss}}. \quad (18)$$

Recalling the definitions of front lateral slip and resultant front slip

$$\frac{s_{Fy}^{\rm ss}}{1+s_{Fx}^{\rm ss}} = \frac{V^{\rm ss}\sin(\beta^{\rm ss}-\delta^{\rm ss}) + V^{\rm ss}\ell_F\cos\delta^{\rm ss}/R^{\rm ss}}{V^{\rm ss}\cos(\beta^{\rm ss}-\delta^{\rm ss}) + V^{\rm ss}\ell_F\sin\delta^{\rm ss}/R^{\rm ss}}, \quad (19)$$

$$s_F^{\rm ss} = \sqrt{(s_{Fx}^{\rm ss})^2 + (s_{Fy}^{\rm ss})^2}, \quad (20)$$

we can numerically solve the system of equations (18), (19) and (20) for the front tire slip quantities s_{Fx}, s_{Fy} and steering angle δ. The steady-state front tire forces f_{Fx} and f_{Fy} are calculated from (7) and (8).

Finally, the steady-state wheel angular rates $\omega_F^{\rm ss}$ and $\omega_R^{\rm ss}$ are calculated using the definition of the longitudinal slip in (5), whereas the torque inputs $T_F^{\rm ss}$ and $T_R^{\rm ss}$ can be obtained from (4) under steady-state conditions.

In Fig. 4 we present cornering equilibria for steady-state path radius of 1 m and 5 m, considering the vehicle and tire model parameters of Table I. In particular, we have plotted the steady-state velocity $V^{\rm ss}$ and the steering angle $\delta^{\rm ss}$, for a range of steady-state vehicle sideslip angles $\beta^{\rm ss}$. In both cases the higher velocity steady-states occur at the highest values of sideslip angle. In the $R^{\rm ss} = 1$ m case the steering angle is along the direction of the corner, and it decreases in magnitude as the magnitude of the sideslip angle increases. In the $R^{\rm ss} = 5$ m case, steady-states are found along a wider range of sideslip angle compared to the $R^{\rm ss} = 1$ m case. In addition, the $R^{\rm ss} = 5$ m steady-states with $\beta^{\rm ss} < -12$ deg require the application of opposite steering angle with respect to the direction of the corner (counter-steering). The stability of the calculated steady-states is determined by linearising the equations of motion (1)-(4) with respect to each equilibrium point. The points marked by 'x' correspond to stable equilibria, and the ones marked by 'o' are unstable. Interestingly, while the majority of the calculated steady-states are unstable, the equilibria in the $R^{\rm ss} = 1$ m case corresponding to $\beta^{\rm ss} < -47$ deg and the highest steady-state velocities are found to be stable. The above brief stability analysis of the equilibria cannot be used to make general conclusions about the stability of handbrake-cornering, as the calculation was performed for a fixed set of vehicle parameters and only a subset of all possible equilibria. Extensive stability analysis of high-sideslip equilibria (for RWD vehicles) appeared in [6] and [9]. In the following we focus on the development of a control architecture to stabilize unstable handbrake-cornering steady-states.

TABLE I

Vehicle Parameters.

m (kg)	1300	r_F r_R (m)	0.28
I_z (kgm^2)	2000	I_{wF} I_{wR} (kgm^2)	1.8
ℓ_f (m)	0.96	B	7
ℓ_r (m)	1.53	C	1.8
h (m)	0.5	D	0.8

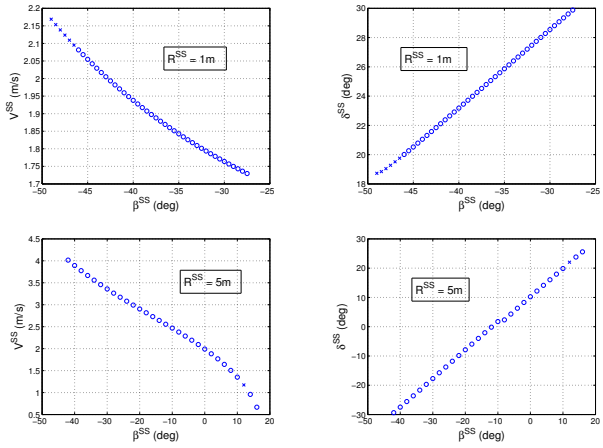

Fig. 4. *Handbrake-cornering equilibria along $R^{\rm ss} = 1$ m and $R^{\rm ss} = 5$ m.*

V. Stabilization of Steady-State Handbrake-Cornering

A control scheme to stabilize a FWD vehicle with respect to handbrake equilibria, using control inputs directly correlating to driver commands, is presented next. The proposed architecture consists of a linear controller providing stabilizing front wheel steering angle (corresponding to the driver's steering command), and front wheel angular rate inputs, assuming locked rear wheels under the application of handbrake. In addition, a backstepping controller calculates the front drive torque (corresponding to the driver's throttle

command) and rear brake torque (corresponding to the driver's handbrake command) necessary to achieve the wheel angular rates dictated by the previous linear controller.

Neglecting the dynamics of each individual wheel rotation (4), the equations of motion of the full-car model (1)-(3), are expressed as a system driven by the steering angle input δ and the reference front wheel angular rate $\hat{\omega}_F$, enforcing $\omega_R = 0$:

$$\dot{V} = f_1(V, \beta, \dot{\psi}, \hat{\omega}_F, \delta), \quad (21)$$

$$\dot{\beta} = f_2(V, \beta, \dot{\psi}, \hat{\omega}_F, \delta), \quad (22)$$

$$\ddot{\psi} = f_3(V, \beta, \dot{\psi}, \hat{\omega}_F, \delta). \quad (23)$$

The equilibrium states $(V^{\rm ss}, \beta^{\rm ss}, \dot{\psi}^{\rm ss})$ and inputs $(\omega_F^{\rm ss}, \delta^{\rm ss})$ are calculated as in Section IV. Equations (21)-(23) are linearized as follows

$$\dot{\mathbf{x}} = \mathbf{A}^{\rm ss}\mathbf{x} + \mathbf{B}^{\rm ss}\mathbf{u} \quad (24)$$

$$\mathbf{y} = \mathbf{C}^{\rm ss}\mathbf{x}, \quad (25)$$

where $\mathbf{A}^{\rm ss}$ and $\mathbf{B}^{\rm ss}$ are the Jacobian matrices, computed at the equilibrium point, and

$$\mathbf{x} = \begin{bmatrix} V - V^{\rm ss} \\ \beta - \beta^{\rm ss} \\ \dot{\psi} - \dot{\psi}^{\rm ss} \end{bmatrix}, \ \mathbf{u} = \begin{bmatrix} \hat{\omega}_F - \omega_F^{\rm ss} \\ \delta - \delta^{\rm ss} \end{bmatrix}, \ \mathbf{C}^{\rm ss} = \mathcal{I}^{3\times 3}.$$

A linear quadratic regulator is designed

$$\mathbf{u} = -\mathbf{K}\mathbf{x}, \quad (26)$$

to stabilize the system (24) with respect to the equilibrium $\mathbf{x} = \mathbf{0}$, using steering angle and front wheel speed inputs.

Next, we design a backstepping controller using the front drive torque T_F and rear brake torque T_R to regulate the rotational speeds of the wheels to the values generated by the control law (26).

The variable z_F is defined as the difference between the actual wheel angular rate ω_F and the reference value $\hat{\omega}_F(\mathbf{x})$:

$$z_F = \omega_F - \hat{\omega}_F(\mathbf{x}), \quad (27)$$

and hence,

$$\dot{z}_F = \dot{\omega}_F - \frac{\partial \hat{\omega}_F(\mathbf{x})}{\partial \mathbf{x}}\dot{\mathbf{x}}. \quad (28)$$

We propose the following backstepping controller, which generates the front wheel torque

$$T_F = T_F^{\rm eq} + I_w v_F, \quad (29)$$

where

$$T_F^{\rm eq} = f_{Fx} r + I_w \left(\frac{\partial \hat{\omega}_F}{\partial V} f_1 + \frac{\partial \hat{\omega}_F}{\partial \beta} f_2 + \frac{\partial \hat{\omega}_F}{\partial \dot{\psi}} f_3 \right) \quad (30)$$

Taking $T_F = T_F^{\rm eq}$ results in $\dot{z}_F = 0$. Equations (28)-(30) yield

$$\dot{z}_F = v_F. \quad (31)$$

Finally, we take

$$v_F = -k_F\, z_F, \quad k_F > 0, \quad (32)$$

which stabilizes (31).

Similarly, we employ a brake torque controller to maintain the rear wheel locked during handbrake-cornering:

$$T_B = f_{Rx} r + I_w v_R, \qquad v_R = -k_R \omega_R, \quad k_R > 0. \quad (33)$$

VI. Simulation Results

In the following we demonstrate the implementation of the control architecture presented in the previous section in the stabilization of unstable handbrake-cornering equilibria. We consider two unstable steady-states: $R^{\rm ss} = 5\,$m, $\beta^{\rm ss} = -42\,$deg, $V^{\rm ss} = 2.05\,$m/sec, and $R^{\rm ss} = 1\,$m, $\beta^{\rm ss} = -45\,$deg, $V^{\rm ss} = 4.02\,$m/sec. In both cases, we consider an initial condition of straight line travel ($\beta = 0$, $\dot{\psi} = 0$) at speed $V = 1.1\, V^{\rm ss}$, and apply the control law (26), (29) and (33). The steering angle input is saturated to a magnitude of $30\,$deg.

The control inputs during stabilization of the $R^{\rm ss} = 5\,$m equilibrium and the corresponding vehicle response are shown in Fig. 5. The dashed lines show the corresponding steady-state values of the vehicle states and control inputs. Figure 7 shows the trajectory of the vehicle during stabilization. We observe that the rear wheel is locked instantaneously, and that the steering angle is initially saturated. The vehicle states are successfully stabilized to their steady-state values after $5\,$sec. The vehicle states and control inputs during stabilization of the $R^{\rm ss} = 1\,$m equilibrium are shown in Fig. 6, and the corresponding trajectory in Fig. 7. The steering angle is saturated during the first $2\,$sec and remains towards the direction of the corner throughout the stabilization of the equilibrium. We may recall that the data presented in Section II also showed no counter-steering during the tight "hairpin" corner. The controller successfully stabilizes the vehicle to the $R^{\rm ss} = 1\,$m steady-state after $4\,$sec.

VII. Conclusions

In this work we studied high-sideslip cornering control for FWD vehicles using the handbrake-cornering technique. Data were collected during the execution of handbrake-cornering maneuvers by an expert race driver and revealed that the technique is used to eliminate vehicle under-steer, as well as to achieve cornering radii considerably lower than the kinematic turning radius. Consequently we examined the existence of high-sideslip cornering equilibria enforcing a FWD configuration of the vehicle model and locked rear wheels under the application of a handbrake control input. The steady-state handbrake-cornering vehicle states and control inputs were computed numerically using a simple single-track vehicle model. The computations revealed that higher cornering velocities are achieved for higher values of sideslip angles. We also observed that the lower radii equilibria may be achieved with a steering command towards the direction of the corner, while higher radii steady-states require counter-steering. The stability of the handbrake-cornering equilibria was assessed via linearization of the equations of motion and a stabilizing backstepping control scheme was developed. The controller designed in this work uses coordinated steering angle and drive/brake torque inputs. Considering that one

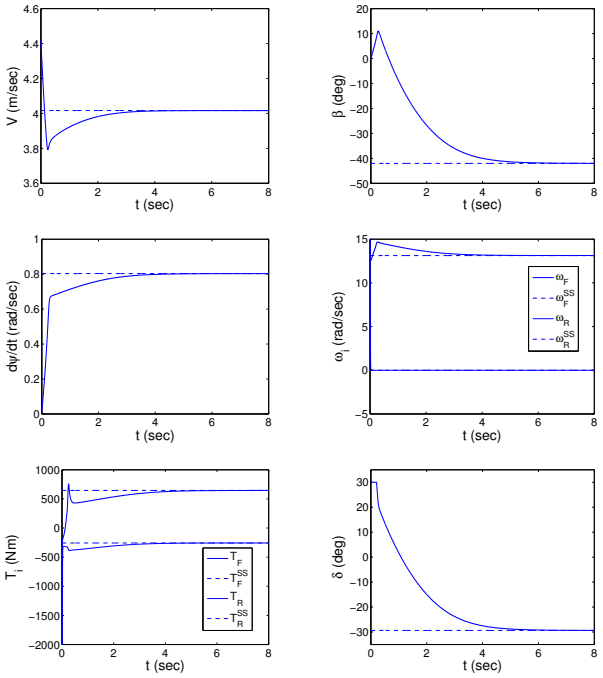

Fig. 5. *Control inputs and vehicle states during stabilization of the $R^{ss} = 5$ m handbrake-cornering equilibrium.*

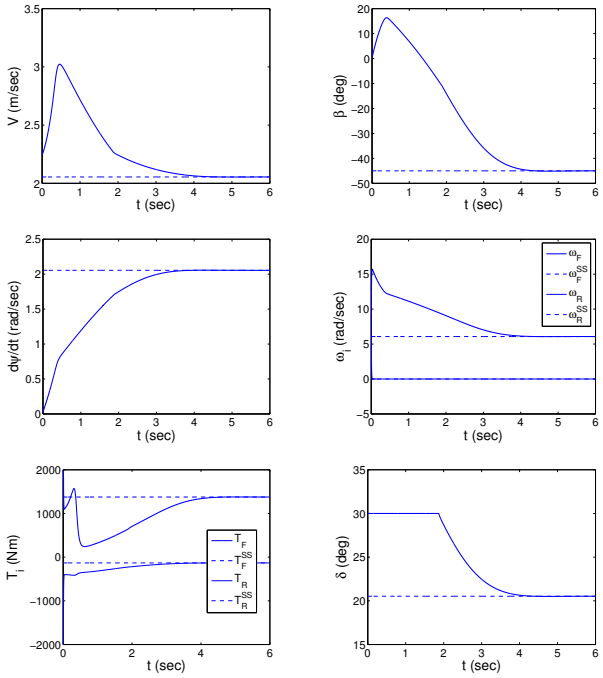

Fig. 6. *Control inputs and vehicle states during stabilization of the $R^{ss} = 1$ m handbrake-cornering equilibrium.*

of the main assumptions in this work is knowledge of the tire force characteristics, the following step of this research will be to implement the control architecture in conjunction with a tire force estimation scheme (for instance [13]). In addition, we plan to extend the control architecture presented herein towards the execution of aggressive transient cornering maneuvers, for instance, negotiating a sequence of corners.

VIII. ACKNOWLEDGMENTS

This work was supported by a Marie Curie International Reintegration Grant within the 7$^{\text{th}}$ European Community Framework Programme and an EPSRC First Grant award (award number EP/I037792/1). The author wishes to thank Mr Bill Gwynne for the insightful discussions on rally driving techniques and his participation in the collection of data as the test driver.

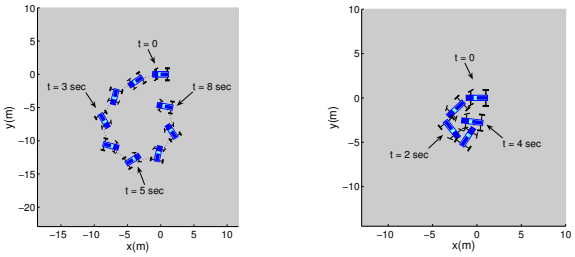

Fig. 7. *Vehicle trajectory during stabilization of the $R^{ss} = 5$ m and $R^{ss} = 1$ m handbrake-cornering equilibria.*

REFERENCES

[1] D. Casanova, R. S. Sharp, and P. Symonds, "Minimum time manoeuvring: The significance of yaw inertia," *Vehicle System Dynamics*, vol. 34, pp. 77–115, 2000.

[2] ——, "On minimum time optimisation of formula one cars: The influence of vehicle mass," in *Proceedings of AVEC 2000*, Ann-Arbor, MI, August 22-24 2000.

[3] E. Velenis, P. Tsiotras, and J. Lu, "Optimality properties and driver input parameterization for trail-braking cornering," *European Journal of Control*, vol. 14, no. 4, pp. 308–320, July-August 2008.

[4] E. Velenis and P. Tsiotras, "Minimum time vs maximum exit velocity path optimization during cornering," in *2005 IEEE International Symposium on Industrial Electronics*, Dubrovnic, Croatia, June 2005, pp. 355–360.

[5] E. Ono, S. Hosoe, H. Tuan, and S. Doi, "Bifurcation in vehicle dynamics and robust front wheel steering control," *IEEE Transactions on Control Systems Technology*, vol. 6, no. 3, pp. 412–420, May 1998.

[6] J. Edelmann and M. Plöchl, "Handling characteristics and stability of the steady-state powerslide motion of an automobile," *Regular and Chaotic Dynamics*, vol. 14, no. 6, pp. 682–692, 2009.

[7] E. Velenis, E. Frazzoli, and P. Tsiotras, "On steady-state cornering equilibria for wheeled vehicles with drift," in *48th IEEE Conference on Decision and Control*, Shanghai, China, December 16-18 2009.

[8] ——, "Steady-state cornering equilibria and stabilization for a vehicle during extreme operating conditions," *International Journal of Vehicle Autonomous Systems, Special Issue on Autonomous and Semi-Autonomous Control for Safe Driving of Ground Vehicles*, vol. 8, no. 2/3, pp. 217–241, 2010.

[9] C. Voser, R. Hindiyeh, and J. Gerdes, "Analysis and control of high sideslip maneuvers," in *21st International Symposium on Dynamics of Vehicles on Roads and Tracks*, Stockholm, Sweden, August 17-21 2009.

[10] E. Velenis, D. Katzourakis, E. Frazzoli, P. Tsiotras, and R. Happee, "Stabilization of steady-state drifting for a rwd vehicle," in *10th International Symposium on Advanced Vehicle Control*, Loughborough, UK, August 22-26 2010.

[11] T. Gillespie, *Fundamentals of Vehicle Dynamics*. Warrendale PA USA: Society of Automotive Engineers SAE International, 1992.

[12] E. Bakker, L. Nyborg, and H. Pacejka, "Tyre modelling for use in vehicle dynamics studies," 1987, SAE Paper No. 870421.

[13] Y. Hsu and J. Gerdes, "The predictive nature of pneumatic trail: Tire slip angle and peak force estimation using steering torque," in *International Symposium on Advanced Vehicle Control*, Kobe, Japan, October 6-9 2008.